Check for updates

ORIGINAL ARTICLE

ORAL DISEASES 🔬 WILEY
Leading in Oral, Maxillofacial, Head & Neck Medicine

Exosomes derived from maxillary BMSCs enhanced the osteogenesis in iliac BMSCs

Xiaobei Li[1] 🆔 | Yunfei Zheng[1] 🆔 | Liyu Hou[2] | Zhibo Zhou[3] | Yiping Huang[1] 🆔 |
Yixin Zhang[1] | Lingfei Jia[3,4] 🆔 | Weiran Li[1] 🆔

[1]Department of Orthodontics, Peking University School and Hospital of Stomatology, Beijing, China

[2]Department of Stomatology, Shenzhen People's Hospital, Shenzhen, China

[3]Department of Oral and Maxillofacial Surgery, Peking University School and Hospital of Stomatology, Beijing, China

[4]Central Laboratory, Peking University School and Hospital of Stomatology, Beijing, China

Correspondence
Weiran Li, Department of Orthodontics, Peking University School and Hospital of Stomatology, 22 Zhongguancun Avenue South, Haidian District, Beijing 100081, China.
Email: weiranli2003@163.com

Lingfei Jia, Department of Oral and Maxillofacial Surgery, Central Laboratory, Peking University School and Hospital of Stomatology, 22 Zhongguancun Avenue South, Haidian District, Beijing 100081, China.
Email: jialingfei1984@sina.com

Abstract

Objective: Secondary alveolar bone grafting is an essential part in the treatment of alveolar cleft deformity. Autologous iliac bone is the most favorable grafting source. However, the factors regulating postoperative bone formation are unclear. Investigations are needed to found whether the alveolar bone niche and bone marrow mesenchymal stem cells (BMSCs) derived from the jaw bone (BMSCs-J) affected the osteogenesis of BMSCs from the ilium (BMSCs-I).

Materials and Methods: The effect of BMSCs-J on BMSCs-I was investigated using a co-culture model. The exosomes were purified by sequential centrifugation. The osteoblastic differentiation of BMSCs was analyzed in vitro and in vivo.

Results: Co-culture with BMSCs-J increased the alkaline phosphatase (ALP) activity, Alizarin Red S (ARS) staining, and osteogenic gene expression in BMSCs-I. Transmission electron microscopy and nanoparticle tracking analysis verified the presence of exosomes in the culture supernatants of BMSCs. Exosomes secreted by BMSCs-J enhanced the ALP activity, ARS staining, osteogenic gene expression of BMSCs-I in vitro, and new bone formation in vivo. Blocking the secretion of exosomes using siRNA for Rab27a inhibited the effect of BMSCs-J.

Conclusion: Exosomes played a role in the interaction between BMSCs-J and BMSCs-I, thereby leading to the enhanced osteogenic capacity of BMSCs-I and bone formation.

KEYWORDS
alveolar bone grafting, exosomes, ilium, jaw, osteogenesis, stem cells

1 | INTRODUCTION

Cleft lip with or without cleft palate is the most common congenital craniofacial deformity, and its prevalence is about 1 per 700

in neonates (Moreau, Caccamese, Coletti, Sauk, & Fisher, 2007). Orofacial clefts have great impact on the quality of life of patients. Over seventy percent of cleft lip and palate cases are accompanied by alveolar cleft (Al-Ahmady et al., 2018). Secondary alveolar bone grafting of the alveolus is an essential part in the treatment of orofacial cleft deformity, which can stabilize the maxillary segments and

Xiaobei Li and Yunfei Zheng are contributed equally to this work.

allow for a spontaneous eruption of canine (Cho-Lee et al., 2013). Autogenous iliac bone grafting is considered the gold standard because of the presence of living immunocompatible bone cells and its strong ability of osteogenesis (Bajaj, Wongworawat, & Punjabi, 2003). However, the factors that affect postoperative bone formation are unclear.

Bone marrow mesenchymal stem cells derived from the ilium (BMSCs-I) possess osteogenic properties and can promote new bone formation and reduce postoperative bone resorption (Ichiyanagi, Anabuki, Nishijima, & Ono, 2010; Ye et al., 2013). Therefore, improving the osteogenesis ability of BMSCs-I might enhance the success rate of bone grafting. The directed differentiation of stem cells is regulated by the surrounding microenvironment (Piecewicz & Sengupta, 2011). From the perspective of embryonic development, the jaw bone is derived from the neural crest, and the iliac is derived from the mesoderm. The gene expression profiles and biological characteristics differ between stem cells derived from a jaw bone defect (BMSCs-J) and BMSCs-I, as does their surrounding microenvironment (Lee et al., 2015). BMSCs-J are involved in the maintenance of alveolar skeletal homeostasis. Thus, when autogenous iliac bone is transplanted into the jawbone defect area, BMSCs-I reside in the maxillary niche which are regulated by BMSCs-J. Although the success rates of implants from iliac and jaw sites were not significantly different, mandibular and calvarial bones grafted for the repair of maxillofacial bone defects presented higher bone volume than iliac bones (Crespi, Vinci, Cappare, Gherlone, & Romanos, 2007; Koole, Bosker, & van der Dussen, 1989). This may be explained by the matching degree of microenvironment and stem cells. However, the effect of the maxillary microenvironment on the properties of BMSCs-I and the intercellular communication between BMSCs-J and BMSCs-I are unclear.

Intercellular communication, a highly conserved cell process, was previously thought to be achieved through either direct cell-to-cell contact or paracrine secretion (Bissell & Radisky, 2001). However, a new mode of intercellular communication mediated by extracellular vesicles, including exosomes, has been a focus of research recently (Mathivanan, Ji, & Simpson, 2010; Thery, Ostrowski, & Segura, 2009). Exosomes are nanovesicles released from a variety of cell types (Record, Carayon, Poirot, & Silvente-Poirot, 2014). They are secreted from intracellular compartments related to late endosomes, known as multivesicular bodies (Bobrie, Colombo, Raposo, & Thery, 2011; Johnstone, Adam, Hammond, Orr, & Turbide, 1987). Emerging evidence indicates that exosomes play an important part in intercellular communication, and specific cell-derived exosomes trigger specific directed differentiation of stem cells (Huang, Narayanan, Alapati, & Ravindran, 2016; Xu et al., 2018; Zhang & Yang, 2018). Exosomes secreted by mineralized preosteoblasts can promote the osteoblast differentiation of BMSCs, suggesting an intercellular communication mediated by exosomes in the osteogenic microenvironment (Cui, Luan, Li, Zhou, & Han, 2016; Fang, Li, & Chen, 2019; Li et al., 2018). Despite much research, the role of exosomes in the intercellular communication between BMSCs-J and BMSCs-I remains unclear.

The increase in the number of bone graft patients necessitates the improvement in the effect of bone graft. To increase the understanding of the crosstalk between BMSCs-J and BMSCs-I in a bone graft setting, we extracted BMSCs-J and BMSCs-I from patients with alveolar cleft and evaluated the effect of BMSCs-J on osteogenesis by BMSCs-I using a co-culture model in this study. We also investigated the effect of exosomes secreted by BMSCs-J on osteogenic ability of BMSCs-I. Our findings may increase the understanding of mechanism underlying the autogenous iliac bone grafting in the alveolar defect area and provide a theoretical foundation for future studies aiming to improve the osteogenic ability of BMSCs-I by regulating intercellular communication.

2 | MATERIALS AND METHODS

2.1 | Cell culture and osteogenic induction

Human BMSCs were isolated separately from the jaw and iliac bones of three donors and cultured as described previously (Guo et al., 2006). The study protocol was approved by the Ethics Committee of Peking University School of Stomatology (PKUSSIRB-201734026). Briefly, a small amount of bone fragments was washed from the surgical equipment during alveolar bone grafting and cut into tiny pieces. The bone tissues were suspended in α-modified Eagle's medium (α-MEM, Gibco) containing 1 mg/ml type II collagenase at 37°C and shaking at a speed of 200 rpm for 60 min. The released blood cells were aspirated, and the bone pieces were incubated in growth medium (GM) containing α-MEM supplemented with 10% fetal bovine serum (FBS, Gibco) and 1% penicillin/streptomycin (Gibco) at 37°C in 5% CO_2. The adherent cells migrated outwards from the bone tissue approximately 1 week later. The cells were passaged using 0.25% trypsin (Gibco) until passage 4 for subsequent experiments.

BMSCs were seeded into six-well plates with cell density of 1.5×10^5/ml. When the cells reached 70%–80% confluence, the induction group was cultured with osteogenic induction medium (OM, containing 10 mM β-glycerophosphate, 200 μM L-ascorbic acid, 100 nM dexamethasone, 10% FBS and α-MEM). The control group was still cultured with GM. The medium was changed every 2 days until the cells were harvested at the indicated time points.

2.2 | Flow cytometry

To evaluate phenotype of BMSCs, the isolated cells were subjected to flow cytometric analysis using a fluorescein isothiocyanate-conjugated monoclonal antibody against human CD90, a phycocyanin-conjugated monoclonal antibody against human CD34, a peridinin chlorophyll protein-conjugated monoclonal antibody against human CD105, and an allophycocyanin-conjugated monoclonal antibody against human CD73 (Becton Dickinson) using the Accuri C6 flow cytometer (Becton Dickinson).

2.3 | Alkaline phosphatase staining and activity

After osteogenic induction for 7 days, ALP staining was performed using a NBT/BCIP staining kit (CoWin Biotech) as described

TABLE 1 The primers used in this study

	Forward	Reverse
GAPDH	5′-CGACAGCAGCCGCATCTT-3′	5′-CCAATACGACCAAATCCGTTG-3′
RUNX2	5′-ACTACCAGCCACCGAGACCA-3′	5′-ACTGCTTGCAGCCTTAAATGACTCT-3′
ALP	5′-GAACGTGGTCACCTCCATCCT-3′	5′-TCTCGTGGTCACAATGC-3′
OSX	5′-CCTCTGCGGGACTCAACAAC-3′	5′-AGCCCATTAGTGCTTGTAAAGG-3′

previously (Huang, Zheng, Jia, & Li, 2015). First, the culture medium was discarded, and then, the cells were gently washed with phosphate-buffered saline (PBS) for 2–3 times. Afterward, cells were fixed in 4% paraformaldehyde for 10 min at room temperature and washed with distilled water. Then, ALP staining was performed following the manufacturer's instructions.

A commercialized ALP activity colorimetric assay kit (BioVision) was used to analyze ALP activity of cells. The cultured cells were washed with cold PBS, then lysed with 1% Triton X-100 (Sigma-Aldrich), and scraped into distilled water. The ALP activity was measured by detecting the absorbance at 405 nm. Total protein concentrations were determined by the bicinchoninic acid (BCA) method using the Pierce protein assay kit (Thermo Fisher Scientific). ALP activity was calculated from the absorbance levels relative to the protein concentration.

2.4 | Alizarin red S staining and quantification

Mineralized nodule formation was determined by ARS staining, as described previously (Zheng, Li, Huang, Jia, & Li, 2017). After osteogenic incubation for 14 days, the cells were fixed in 4% paraformaldehyde for 10 min and then stained with 0.1% ARS (pH 4.2; Sigma-Aldrich) for 20 min at room temperature. To quantitatively evaluate the mineralized nodules, the stain was dissolved in 1 ml 10% cetylpyridinium chloride (Sigma-Aldrich) for 1 hr and the absorbance at 570 nm was detected by spectrophotometric methods. The intensity of ARS was normalized to the total protein concentration.

2.5 | RNA extraction and quantitative reverse-transcription polymerase chain reaction

Total RNA was extracted using TRIzol reagent (Invitrogen) according to the manufacturer's procedure. Total RNA (1 μg for each sample) was reverse-transcribed into cDNA using a cDNA Reverse Transcription Kit (Applied Biosystems). Quantitative reverse-transcription polymerase chain reaction (qRT-PCR) was conducted using SYBR Green Master Mix on the ABI Prism 7500 Real-Time PCR System (Applied Biosystems). The primers used for *ALP*, osterix (*OSX*), runt-related transcription factor 2 (*RUNX2*), and glyceraldehyde 3-phosphate dehydrogenase (*GAPDH*, internal control) are listed in Table 1. The Ct (Cycle threshold) value of each gene was detected. The relative expression level of the tested genes was evaluated by $2^{-\Delta\Delta CT}$ method as described previously (Huang, Zheng, et al., 2016).

2.6 | Immunofluorescence staining

Cells cultured on cover slips were fixed with 4% paraformaldehyde and then subjected to immunofluorescence staining. The mouse skull specimens were decalcified, embedded, and cut into sections for staining. Immunofluorescence staining was performed as described previously (Zheng et al., 2016). The cells or specimens were blocked with 3% goat serum albumin (ZSGB-BIO) for 30 min at room temperature and then incubated with the appropriate primary antibodies at 4°C overnight. Then, cells or sections were incubated with the corresponding secondary antibodies for 1 hr at room temperature. Nuclei were counterstained with 4',6-diamidino-2-phenylindole (DAPI). After sealing, images were captured with a LSM 5 EXCITER confocal imaging system (Carl Zeiss).

2.7 | Co-culture of BMSCs-J and BMSCs-I

BMSCs-J and BMSCs-I were co-cultured in a transmembrane system (Transwell, Corning) with 0.4 μm pore-size filters as described previously (Gao, Connell, Wadhwa, Ruano, & Jacot, 2014). BMSCs-I were seeded on the bottom of the lower well of the Transwell plate. In group I, BMSCs-I were seeded into the upper chamber with cell density of 5×10^4/ml. In group II, BMSCs-J were seeded into the upper chamber with cell density of 5×10^4/ml. In group III, BMSCs-J were seeded into the upper chamber with cell density of 2×10^4/ml (Figure 2a). Due to the limitation of pore size, the membrane allows biomacromolecules, but not cells, to pass through the micropores. Thus, a noncontact co-culture system of BMSCs-J and BMSCs-I was established.

2.8 | Exosome purification and characterization

Exosomes were purified by sequential centrifugation as described previously (Baglio et al., 2015). First, cells were cultured in α-MEM supplemented with 10% exosome-depleted FBS (Gibco). Then, the culture supernatant was collected and the cells were removed by centrifugation at 500 g for 10 min. Thereafter, the supernatants were centrifuged at 12,000 g for 20 min to remove apoptotic bodies and large cell debris. Finally, exosomes were collected by centrifugation at 100,000 g for 70 min.

The collected vesicles were resuspended in PBS and characterized by transmission electron microscopy (TEM) as described previously (Jiang et al., 2017). Briefly, exosome samples were fixed with 2% paraformaldehyde and loaded on parafilm.
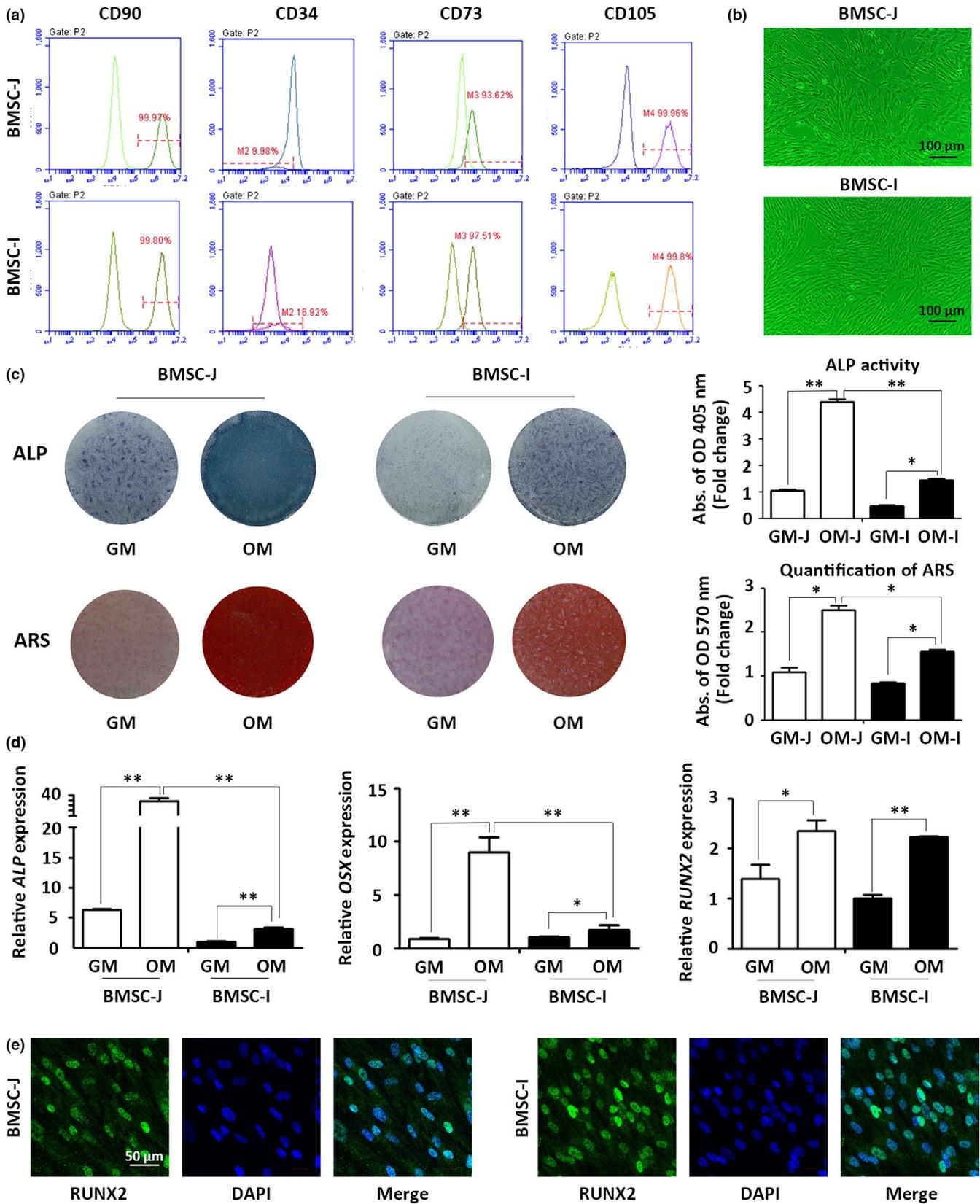
A formvar–carbon-coated grids were placed on the samples for 20 min. The grids were washed, and exosomes were stained with 2% uranyl acetate. After washing and air drying, the samples were examined by TEM (JEM-1400) at 100 KV.

Exosomes were diluted to PBS for size measurement by nanoparticle tracking analysis (NTA) as previously reported protocol (Kalimuthu et al., 2018). The samples were resuspended and added into the viewing chamber of NanoSight LM10 (Particle

FIGURE 1 The surface markers and the osteogenic potential of bone marrow mesenchymal stem cells (BMSCs) derived from a jaw bone defect (BMSCs-J) and BMSCs derived from the ilium (BMSCs-I). (a) The isolated BMSCs were positive for the mesenchymal stem cell markers CD90, CD73, and CD105 and negative for the hematopoietic stem cell marker CD34. (b) The light field images showed that the BMSCs exhibited a fibroblast-like morphology. (c) The images of alkaline phosphatase (ALP) and Alizarin Red S (ARS) staining of BMSCs were shown at growth medium (GM) group and osteogenic medium (OM) group. Histograms showed ALP activity and quantification of ARS staining by spectrophotometry. (d) Relative mRNA expression of *ALP, osterix (OSX)*, and *runt-related transcription factor 2 (RUNX2)* was increased during osteogenic differentiation (by qRT-PCR; normalized by glyceraldehyde 3-phosphate dehydrogenase (GAPDH); relative to GM groups). (e) Confocal microscopy of RUNX2 with DAPI counterstaining in BMSCs-J and BMSCs-I after induction to the osteogenic lineage at day 14. *$p < .05$ compared to GM groups. **$p < .001$ compared to GM groups

Characterization Laboratories). The NTA software was used to track and measure the size of exosomes.

Western blot analysis was conducted to measure the exosome proteins. Total proteins extracted from cell lysates and secreted extracellular vesicles were separated by 12% sodium dodecyl sulfate–polyacrylamide gel electrophoresis and transferred to polyvinylidene difluoride (PVDF) membranes (Millipore). Then, the PVDF membranes were blotted with primary antibodies against CD63 (1:500, Santa Cruz Biotechnology), Alix (1:250, Santa Cruz Biotechnology), and GM130 (1:250, BD Bioscience) overnight at 4°C. After three washes with TBST, the PVDF membranes were incubated with corresponding secondary antibodies (1:10,000, Cell Signaling Technology) for 1 hr at room temperature. After three washes with TBST, the PVDF membranes were incubated with the chemiluminescent reagent (Solarbio). Then, images were captured by the gel imaging system.

2.9 | Transfection assay

Transfection was conducted when cells reached 70%–80% confluence using Lipofectamine 3000 (Invitrogen) according to the manufacturer's protocol. The RNA oligoribonucleotides, including the small interfering RNAs (siRNAs) targeting Rab27a and the corresponding siRNA control (si-NC), were purchased from GenePharma Co. The RNA oligoribonucleotides were transfected separately at 100 nM. Western blot analysis was conducted to measure the transfection efficiency. The primary antibodies against Rab27a (1:500, Santa Cruz Biotechnology) and β-ACTIN (1:1000, Santa Cruz Biotechnology, internal control) were used.

2.10 | In vivo bone formation assay

The critical-sized mouse calvarial defect model was constructed as previously described (Cooper et al., 2010; Krebsbach, Mankani, Satomura, Kuznetsov, & Robey, 1998). The animal experimental protocols were approved by the Laboratory Animal Rights and Ethics Management Committee of Peking University Medical Department (LA2018305). The operation was performed on 60-day-old adult male nude mice (BALB/c) under general anesthesia. After gently removing the pericranium, non-healing, critical-sized calvarial defects (4 mm in diameter) were created using a sterile dental drill. The drill penetrated the whole skull layer without damaging the dura mater. The operation area was washed with sterile saline, and debris of residual bone tissue was removed. We used poly lactic-co-glycolic

acid (PLGA; Melone) as scaffold material. The scaffolds were prepared as thin circular slices approximately 4 mm in diameter. The cells were seeded in the scaffold material and then gently implanted into the mouse skull defect area. The skin incision was closed with 5–0 Vicryl sutures. After 12 weeks, the skull tissues of animals were harvested and fixed in 4% polyoxymethylene at 4°C for subsequent experiments.

2.11 | Micro-computed tomography analysis

The skull specimens were scanned by a high-resolution Inveon Micro-CT (Siemens) to measure new bone formation. All samples were placed in the same container and scanned with uniform parameters. The scanning parameters were set at an effective pixel size of 8.99 μm, voltage of 80 kV, current of 500 μA, and exposure time of 1,500 ms. The specimens were scanned through a 360° rotation in 360 equiangular steps. Three-dimensional images were reconstructed using Inveon Research Workplace 3.0 software (Siemens). Relevant parameters of new bone formation, including bone mineral density (BMD, mg/ml) and the ratio of new bone volume to existing tissue volume (BV/TV), were calculated.

2.12 | Histological analysis

The fixed skull specimens were flushed with water and then decalcified in 10% ethylene diamine tetraacetic acid (EDTA, pH = 7.4) for 1 month, as previously described (Herberg et al., 2014).The EDTA solution was changed every 2 days until the needle could penetrate the specimens without resistance. The specimens were then washed, dehydrated, and embedded in paraffin. Sections were cut at 7 μm and subjected to standard hematoxylin and eosin (H&E) staining. The images were captured using an Olympus BX51 light microscope equipped with an Olympus DP70 camera (Olympus Co.). Sections were also assessed by immunofluorescence analysis, as mentioned above.

2.13 | Statistical analysis

Quantitative data are expressed as means ± standard deviation (*SD*) of at least three independent experiments, unless otherwise indicated. The significance of the differences was evaluated by one-way analysis of variance followed by the Student–Newman–Keuls post hoc test using SPSS 16.0 software (SPSS). *p* Value <.05 was considered indicative of statistical significance.

3 | RESULTS

3.1 | Identification and osteogenic differentiation of BMSCs

The isolated BMSCs migrated from the jaw and iliac bones after approximately 7 days, and their surface expression profile was evaluated by flow cytometry. The BMSCs were positive for the mesenchymal stem cell markers CD90, CD73, and CD105 and negative for the hematopoietic stem cell marker CD34 (Figure 1a). The BMSCs exhibited a fibroblast-like morphology, and no clear morphological differences were identified between BMSCs-J and BMSCs-I (Figure 1b). Following incubation in osteogenic medium for 7 days, the staining and activity of ALP staining were increased significantly. Similarly, the intensity of ARS staining was significantly increased after induction for 14 days (Figure 1c, the separate data of other two samples were shown in Figure S1). Besides, the intensities of ALP and ARS staining of BMSCs-J were greater than that of BMSCs-I ($p < .05$). Furthermore, osteogenic differentiation of BMSCs was assessed by measuring osteogenic markers using qRT-PCR and immunofluorescence. The results of qRT-PCR revealed that the mRNA expression of *ALP*, *OSX*, and *RUNX2* was significantly increased after osteogenic induction in both BMSCs-J and BMSCs-I, while the expression level of these markers was higher in BMSC-J compared to BMSCs-I ($p < .05$; Figure 1d). Meanwhile, RUNX2 was highly expressed in the induced BMSCs as revealed by immunofluorescence staining (Figure 1e). Collectively, these results indicated that the osteogenic capacity of BMSCs-J was greater than that of BMSCs-I.

3.2 | Co-culture with BMSCs-J promotes osteogenic differentiation of BMSCs-I

Co-culture of BMSCs-J and BMSCs-I was performed to simulate their interaction in vitro (Figure 2a). After osteogenic induction for 7 days, the ALP staining intensity of BMSCs-I was increased when co-cultured with BMSCs-J. Meanwhile, the intensity of ARS staining was also increased in group II and group III following osteogenic induction for 14 days, indicating an enhancement of mineralized nodule formation of BMSCs-I. However, the ALP and ARS staining intensities were decreased when the number of BMSCs-J was reduced in group III (Figure 2b, the separate data of other two samples were shown in Figure S2). Furthermore, the results of qRT-PCR showed that the mRNA expression of osteogenic markers, such as *ALP*, *OSX*, and *RUNX2*, in BMSCs-I was upregulated by co-culture with BMSCs-J. Likewise, reducing the number of BMSCs-J weakened this effect (Figure 2c).

3.3 | Isolation and characterization of exosomes

Exosomes isolated from BMSCs-J and BMSCs-I culture supernatants were analyzed by TEM and NTA to verify their purification. TEM revealed that the BMSCs-J and BMSCs-I secrete ~100 nm ring-like vesicles (Figure 3a). The exosomes had a complete membrane structure containing a low-density substance. NTA indicated the presence of ~100 nm cellular particles in cultured BMSCs-J and BMSCs-I (Figure 3b), consistent with the size of exosomes. The isolated exosomes were positive for the extracellular vesicles marker Alix and CD63, but negative for the Golgi marker GM130, suggesting the absence of Golgi or cell contamination (Figure 3c). The exosomes extracted from the two cell types were not significantly different in appearance and size.

3.4 | BMSC-J exosomes promote osteogenic differentiation of BMSCs-I

The purified exosomes secreted by BMSCs-J and BMSCs-I were collected. We also collected the exosomes of BMSC-J after blocking the exosome secretion with siRNA for Rab27a. In group I, exosomes secreted by BMSCs-I were added to the culture medium as a control. In group II, exosomes secreted by BMSCs-J were added to the culture medium of BMSCs-I. Accordingly, the exosomes of BMSC-J after blocking the exosome secretion with siRNA for Rab27a were added to the culture medium in group III (Figure 4a). Western blot analysis confirmed that the expression of Rab27a was decreased in the knockdown group (Figure 4b). After osteogenic induction for 7 days, the intensity of ALP staining was increased in group II and III compared to the control group. However, the intensity of ALP staining was decreased in group III compared to group II. Similarly, the matrix mineralization was also increased in group II and III compared with the control group after osteogenic induction for 14 days, as revealed by ARS staining. And the intensity of ARS staining was decreased in group III compared to that of group II (Figure 4c, the separate data of other two samples were shown in Figure S3). Moreover, the *ALP*, *OSX*, and *RUNX2* expression levels in BMSCs-I were upregulated in group II and III compared with the control group; however, it was much higher in group II (Figure 4d). These results indicated that exosomes secreted by BMSCs-J promoted the osteoblast differentiation of BMSCs-I.

3.5 | BMSCs-J exosomes promote bone formation of BMSCs-I in vivo

To further verify the role of exosomes secreted by BMSCs-J in osteoblast differentiation of BMSCs-I, we conducted animal experiments in vivo (Figure 5a). In group I, scaffold material was loaded with neither cells nor exosomes. In group II, BMSCs-I were cultured in the medium containing exosomes secreted by BMSCs-I. Following cultured for 7 days, the cells were digested using trypsin and then loaded on scaffold material. In group III, BMSCs-I were cultured in the medium containing exosomes secreted by BMSCs-J. Following cultured for 7 days, the cells were loaded to scaffold material. In group IV, scaffold material was only loaded with exosomes secreted by BMSCs-I (exosome-I). Accordingly, scaffold material was only loaded with exosomes secreted by BMSCs-J (exosome-J) in group V. The scaffolds were then gently implanted in the calvarial defect area of nude mice. After 12 weeks, the mice were sacrificed and skull specimens were harvested for further studies. Three-dimensional reconstructed micro-CT images were used to visualize the repair of bone defects. More bone formation and smaller range of bone defect were observed in group II and group III

FIGURE 2 The co-culture of BMSCs-J and BMSCs-I. (a) Scheme for the co-culture of BMSCs-J and BMSCs-I in vitro. BMSCs-I were seeded on the bottom of the lower dish of the Transwell plate. In group I, BMSCs-I were seeded into the upper chamber with cell density of 5×10^4/ml. In group II, BMSCs-J were seeded into the upper chamber with cell density of 5×10^4/ml. In group III, BMSCs-J were seeded into the upper chamber with cell density of 2×10^4/ml. (b) The images of ALP and ARS staining of BMSCs were shown in three groups. Histograms showed ALP activity and quantification of ARS staining by spectrophotometry. (c) Relative mRNA expression of *ALP*, *OSX*, and *RUNX2* in three groups (by qRT-PCR; normalized by GAPDH; relative to group I). *$p < .05$. **$p < .001$
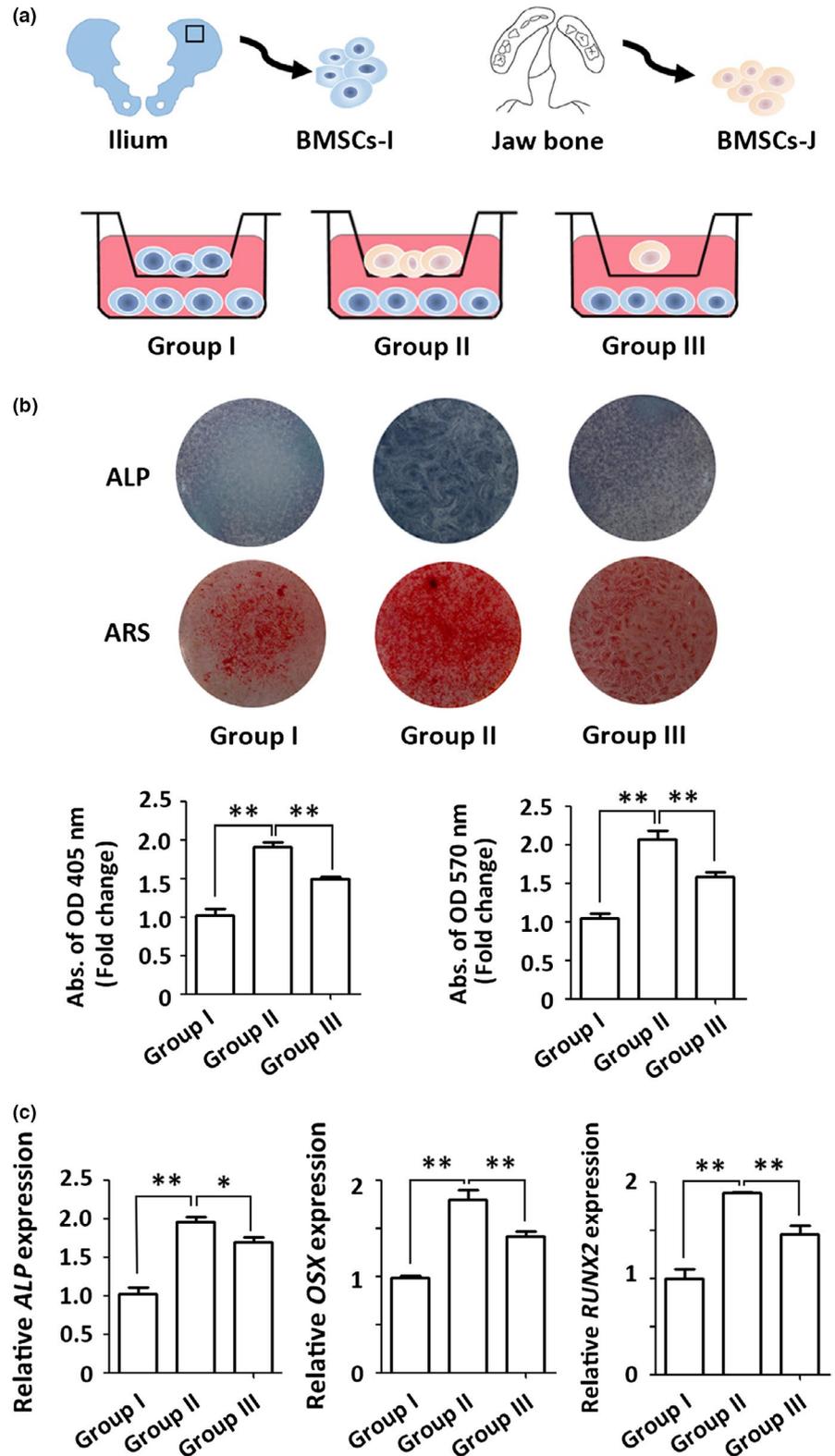
compared to the control group. Besides, more bone formation was seen in group III than group II. The BMD and BV/TV were significantly increased in group III. In addition, more bone formation was observed in the exosome-loaded groups (group IV and V) compared to the negative control group; however, there was no significant difference between the two exosome-loaded groups. Furthermore, new bone formation of two exosome-loaded groups was significantly less than that of the cell-loaded groups (groups II and III; Figure 5b). Consistently, H&E staining showed new bone formation around the bone defect areas in both exosome-loaded groups and cell-loaded groups. However, there was a more active bone repair trend and more new bone formation in cell-loaded groups. And more new bone formation was observed in group

(a)

**BMSC-J exosome**   **BMSC-I exosome**
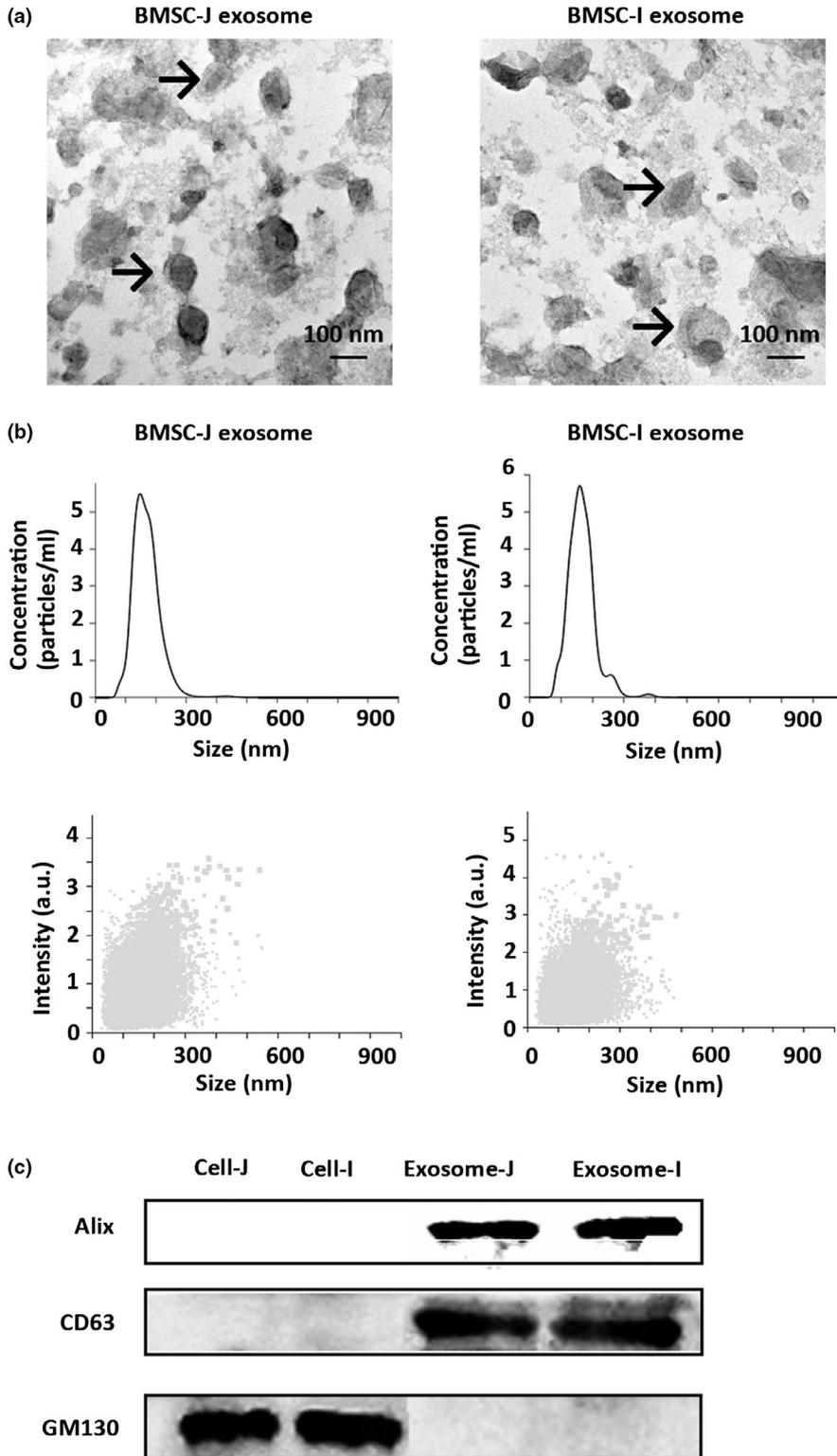
FIGURE 3 Characterization of exosomes. (a) Transmission electron microscopy (TEM) revealed that the BMSCs-J and BMSCs-I secrete ~100 nm vesicles. The arrows indicated the exosomes. (b) Nanoparticle tracking analysis (NTA) showed the presence of ~100 nm cellular vesicles in cultured BMSCs-J and BMSCs-I. (c) Total proteins extracted from nanometer vesicles and parent cells probed by anti-Alix, anti-CD63, and anti-GM-130 antibodies

(b)

(c)

III compared to group II (Figure 5c). Moreover, immunofluorescence staining showed that the bone tissue was positive for RUNX2 staining, whereas the staining intensity in group III was stronger than that in group II (Figure 5d). These results suggested that exosomes produced by BMSCs-J enhanced the osteogenic capacity of BMSCs-I in vivo. Besides, BMSCs play a more important role in bone formation while exosomes partially promote this process.

4 | DISCUSSION

Patients with a maxillary alveolar cleft often require alveolar bone grafting to stabilize the dental arch and enable eruption of the permanent teeth into the grafted area (Benlidayi, Tatli, Kurkcu, Uzel, & Oztunc, 2012). Autologous iliac bone grafts are the gold standard for alveolar reconstruction (Mikoya et al., 2010; Nwoku, Al Atel, Al
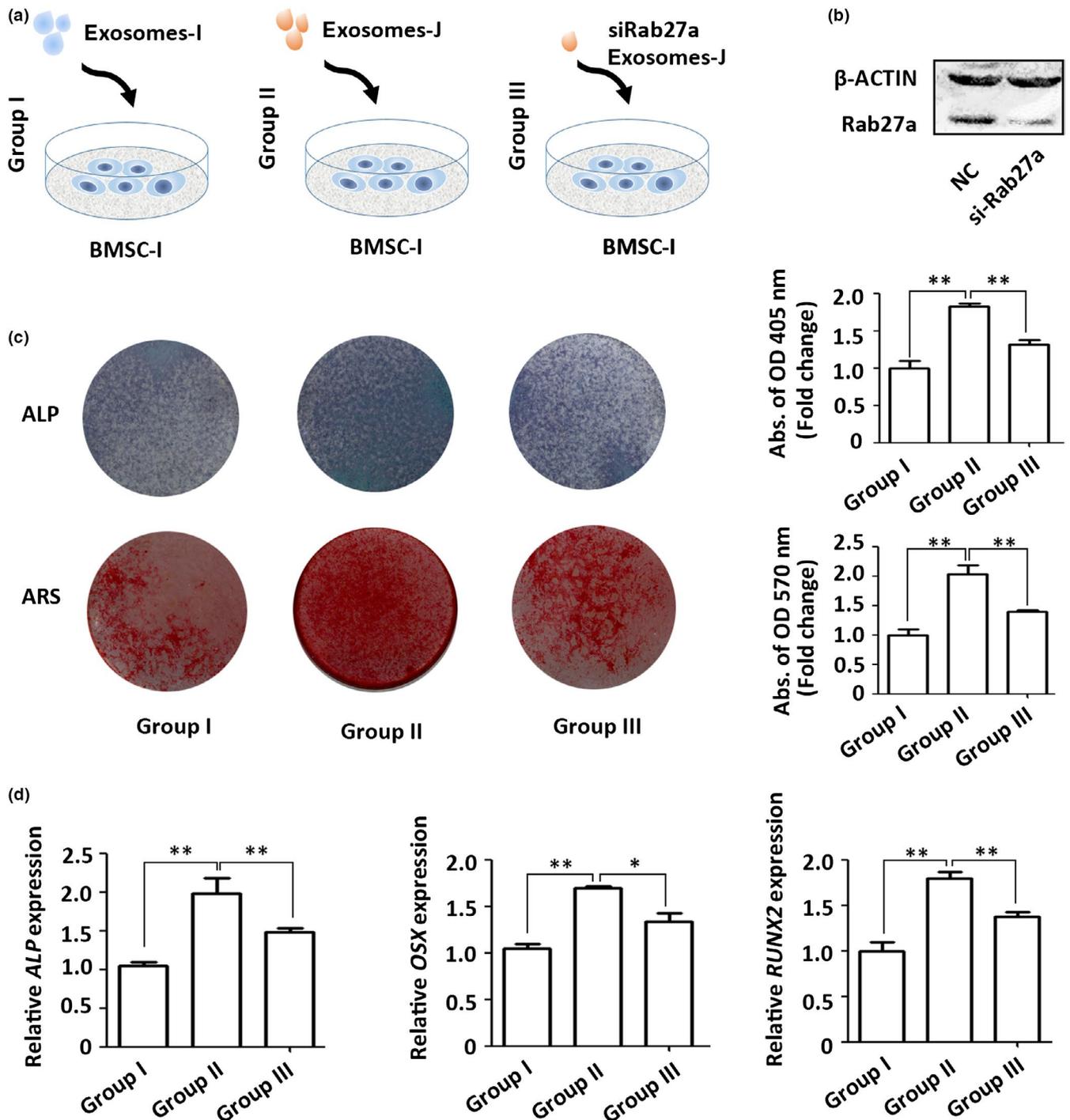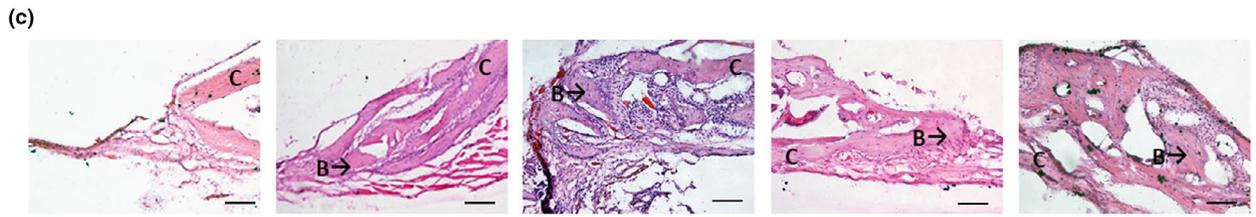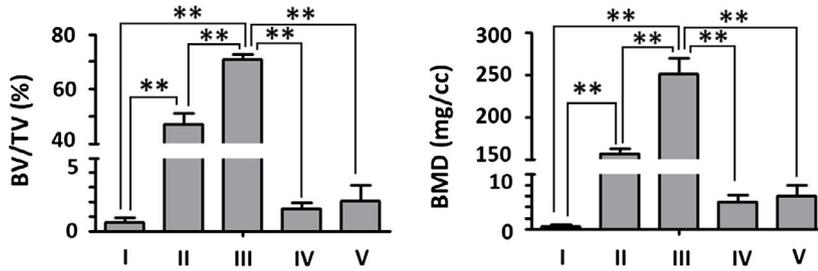
FIGURE 4 Exosomes secreted by BMSCs-J promote osteogenic differentiation of BMSCs-I. (a) The schema chart explained the grouping method. In group I, exosomes secreted by BMSCs-I (exosome-I) were added to the culture medium of BMSCs-I as a control. In group II, exosomes secreted by BMSCs-J (exosome-J) were added to the culture medium. In group III, the exosomes of BMSC-J after blocking the exosome secretion with siRNA for Rab27a (siRab27a exosome-J) were added to the culture medium. (b) The knockdown efficiency of si-Rab27a detected by Western blot. (c) The images of ALP and ARS staining of BMSCs were shown at three groups. Histograms showed ALP activity and quantification of ARS staining by spectrophotometry. (d) Relative mRNA expression of *ALP*, *OSX*, and *RUNX2* in three groups (by qRT-PCR; normalized by GAPDH; relative to group I). *$p < .05$. **$p < .001$

Shlash, Oluyadi, & Ismail, 2005), as they are immunologically inert and potentially supply cells with osteogenic, osteoconductive, and osteoinductive properties, such as BMSCs-I, to facilitate bone healing (Gimbel et al., 2007). The differentiation of stem cells is regulated

by the surrounding microenvironment (Piecewicz & Sengupta, 2011). In vivo experiments show that transplanted MSCs can differentiate into cells similar to their surrounding cells in the tissue microenvironment (Mimeault, Hauke, & Batra, 2007). Transplantation of
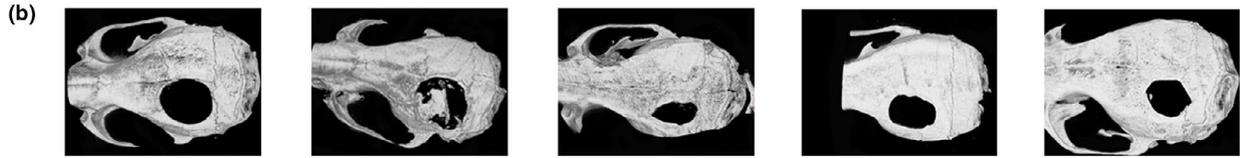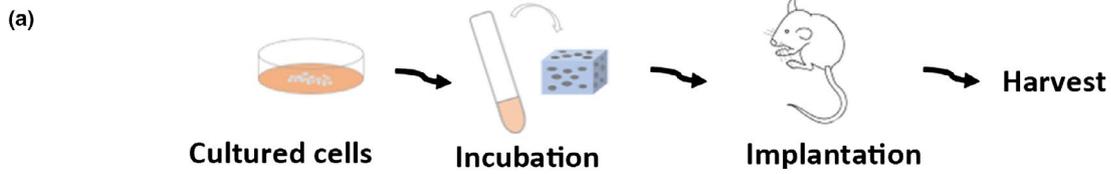
(a)

Cultured cells → Incubation → Implantation → Harvest

(b)

I: Negative control   II: BMSC-I + exo-I   III: BMSC-I + exo-J   IV: Exo-I   V: Exo-J

(c)

I: Negative control   II: BMSC-I + exo-I   III: BMSC-I + exo-J   IV: Exo-I   V: Exo-J

(d)

RUNX2

DAPI

Merge
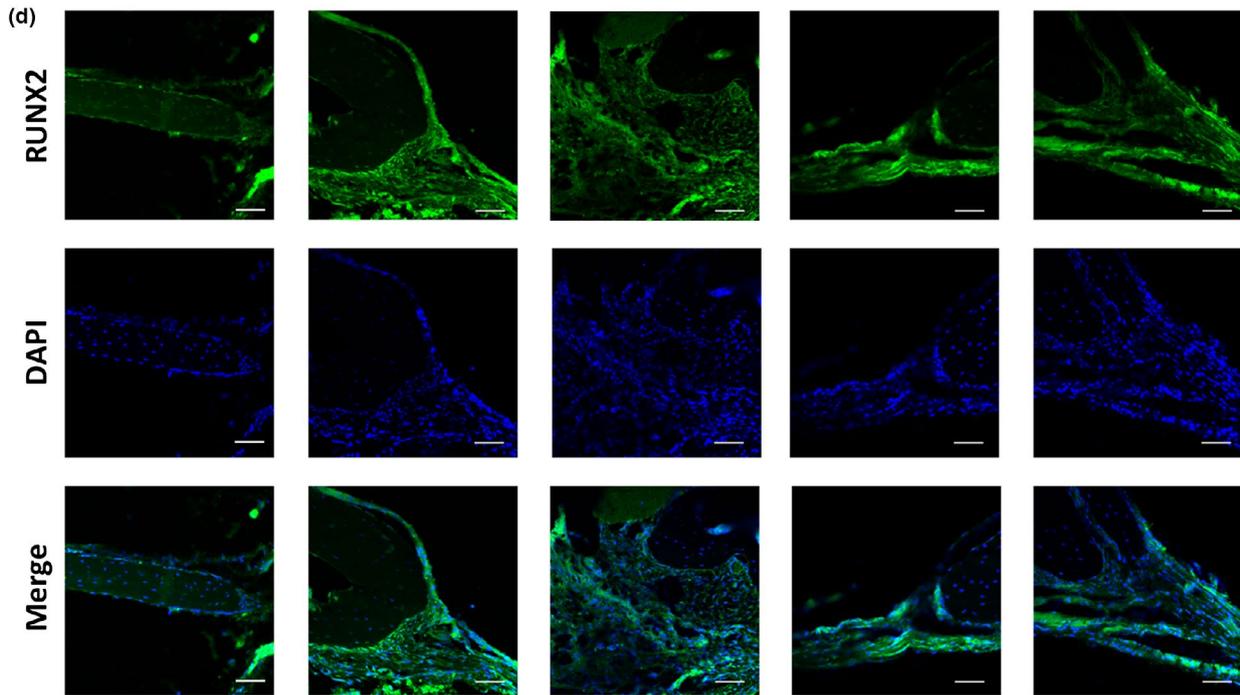
I: Negative control   II: BMSC-I + exo-I   III: BMSC-I + exo-J   IV: Exo-I   V: Exo-J

FIGURE 5 Exosomes secreted by BMSCs-J promoted bone formation of BMSCs-I in vivo. (a) Schematic illustration showed the protocol of animal experiments. (b) Reconstructed three-dimensional micro-CT images of the calvarial defect area of nude mice in five groups. In group I, scaffold material was loaded with neither cells nor exosomes. In group II, scaffold material was loaded with BMSCs-I cultured with exosomes secreted by BMSCs-I (exo-I). In group III, scaffold material was loaded with BMSCs-I cultured with exosomes secreted by BMSCs-J (exo-J). In group IV, scaffold material was loaded with exo-I. In group V, scaffold material was loaded with exo-J. The histograms showed the bone mineral density (BMD, left) and the ratio of new bone volume to existing tissue volume (BV/TV, right) of five groups. (c) H&E staining in five groups. Bone formation (b) around the original cranial bones (c) was identified. Scale bar, 100 μm. (d) Confocal microscopy of RUNX2 with DAPI counterstaining in five groups in the calvarial defect area. Scale bars, 50 μm. *$p < .05$. **$p < .001$

autogenous iliac bone into the jawbone defect area influences both the BMSCs-I microenvironment and local intercellular communication (Lee et al., 2015). Thus, BMSCs-I may be regulated by BMSCs-J in the bone defect area, which affects their properties. However, it is controversial whether BMSCs-J exhibit osteogenic properties superior to BMSCs-I (Akintoye et al., 2006; Lee et al., 2015; Matsubara et al., 2005), and the interaction between BMSCs-J and BMSCs-I in iliac cancellous bone grafting is unclear.

In our study, we extracted BMSCs-J and BMSCs-I from patients with cleft lip and palate and evaluated their interaction in terms of osteoblast differentiation. To evaluate the characteristics of the cells, we performed osteogenic induction culture. Osteoblastic differentiation evaluated by ALP activity and ARS staining in BMSCs-J was stronger than that in BMSCs-I, which is consistent with previous reports (Akintoye, Giavis, Stefanik, Levin, & Mante, 2008; Akintoye et al., 2006). Another report showed that alveolar and iliac BMSCs display similar osteogenic potential (Matsubara et al., 2005). However, Lee et al. reported that in vitro ALP activity was higher in iliac BMSCs than in mandibular BMSCs (Lee et al., 2015), using bone cells from elderly patients (60.2 ± 4.6 years of age). Jaw and long bone marrow cells exhibit different characteristics in terms of osteoblastic differentiation and osteoclastogenesis in vitro and bone formation in vivo (Aghaloo et al., 2010; de Souza Faloni et al., 2011). The differences might be attributed to embryological divergence and the differences between the two sites. MSCs from maxillary and mandibular alveolar and basal bones originate from neural crest cells and exhibit intramembranous bone formation (Chai & Maxson, 2006), whereas MSCs from bones of the axial skeleton, such as the ilium or tibia, originate from the mesoderm and undergo endochondral bone formation (Helms & Schneider, 2003). Moreover, the differentiation of neural crest stem cells and BMSCs from the mesoderm is regulated by different genes (Chai et al., 2000; Mackie, Ahmed, Tatarczuch, Chen, & Mirams, 2008). Alternatively, the cellular characteristics of alveolar and basal mandibular bone may not be identical (Lee et al., 2015), even though both bones are of neuroectodermal origin.

To investigate the interaction between BMSCs-J and BMSCs-I, we performed Transwell co-culture in vitro. The osteogenic capacity of BMSCs-I was enhanced when co-cultured with BMSCs-J. Transwell film is a type of polyester material with a diameter of ≤3 μm. The membrane allows biomacromolecules, but not cells, to pass through the micropores; this facilitates co-culture without cell-to-cell contact (Barbero-Becerra et al., 2015). Upon co-cultured with BMSCs-J, *ALP*, *OSX*, and *RUNX2* expression was increased in BMSCs-I, suggesting an enhanced osteogenic capacity. Moreover, reducing the number of BMSCs-J weakened this promoting effect of

BMSCs-I. Thus, bioactive molecules secreted by BMSCs-J may upregulate the osteogenic capacity of BMSCs-I.

Furthermore, we found exosomes produced by BMSCs-J enhanced the osteogenic capacity of BMSCs-I. Exosomes are nanosized extracellular vesicles released from a variety of cell types. Following release, exosomes can be taken up by target cells in the local microenvironment or transported to distal sites via biological fluids (Baglio et al., 2015). In this study, we extracted exosomes secreted by BMSCs-J and BMSCs-I. The isolated vesicles were confirmed to be exosomes by electron microscopy analyses, particle size, and Western blot analyses. Our findings suggest that the osteogenic differentiation of BMSCs-I was enhanced when they were cultured in medium containing exosomes derived from BMSCs-J. This is consistent with the results of co-culture assays. To further confirm the effect of exosomes secreted by BMSCs-J on BMSCs-I, we blocked the exosome secretion process of BMSCs-J by siRNA targeting Rab27a. Rab27a is an important protein in the process of exosome secretion (Ostrowski et al., 2010). Several studies demonstrated that knockdown of Rab27a can effectively inhibit exosome secretion (Lan et al., 2019; Ostrowski et al., 2010; Poggio et al., 2019). Our results showed that blocking exosome secretion of BMSCs-J weakened its promoting effect on BMSCs-I, as revealed by ALP staining, ARS staining, and expression of osteogenic genes. These results indicated that exosomes secreted by BMSCs-J promoted the osteoblast differentiation of BMSCs-I. Meanwhile, the results of in vivo study further confirmed that the exosomes secreted by BMSCs-J could enhance the bone formation capacity of BMSCs-I. However, new bone formation of two exosome-loaded groups was significantly less than that of the cell-loaded groups. Therefore, exosomes played a role in the interaction between BMSCs-J and BMSCs-I as a regulatory factor, thereby upregulating the osteogenic capacity of BMSCs-I. Besides, BMSCs play a more important role in bone formation while exosomes partially promote this process.

Exosomes mediate intercellular signaling in a variety of biological processes (Kim et al., 2005). Exosomes can transport proteins, lipids, and nucleic acids, especially various RNA species with regulatory functions (Valadi et al., 2007). It is generally believed that the contents of exosomes exert biological effects. Exosomes derived from mineralizing preosteoblasts promote bone marrow stromal cell differentiation into osteoblasts, suggesting an exosome-mediated mode of cell-to-cell communication in the osteogenic microenvironment (Cui et al., 2016; Fang et al., 2019; Li et al., 2018). Therefore, the exosomes secreted by BMSCs-J might regulate the osteogenesis of BMSCs-I by transmitting some signal molecules such as proteins or non-coding RNAs. However, we did not identify the active

component(s) in this study, and thus, further research is needed to explore this underlying mechanism.

In summary, we found that the osteogenic capacity of BMSCs-I was enhanced by co-culture with BMSCs-J or exposure to the exosomes derived from BMSCs-J in vitro and in vivo. Our findings may increase the understanding of mechanism underlying the autogenous iliac bone grafting in the jaw and facilitate future studies on the osteogenic capacity of transplanted BMSCs-I. However, further assessment of the specific underlying mechanism is needed.

ACKNOWLEDGEMENTS

CONFLICT OF INTEREST

The authors have no conflicts of interest to declare.

AUTHOR CONTRIBUTIONS

X.L. involved in conception and design and data acquisition, analyzed and interpreted the data, and contributed to writing of the manuscript; YF.Z. involved in conception and design and data acquisition, and contributed to writing of the manuscript; L.H. and Z.Z. involved in conception and design and data acquisition; Y.H. and YX.Z. involved in data acquisition; L.J. involved in conception and design, analyzed and interpreted the data, and contributed to writing of the manuscript; and W.L. involved in conception and design, gave financial support, and revised the manuscript. All authors approved the final version of the manuscript. X.L. and Y.Z. contributed equally to this work.

ORCID

Xiaobei Li https://orcid.org/0000-0003-2913-6895

Yunfei Zheng https://orcid.org/0000-0003-1899-8051

Yiping Huang https://orcid.org/0000-0002-9230-1825

Lingfei Jia https://orcid.org/0000-0002-1227-1233

Weiran Li https://orcid.org/0000-0001-9895-1143

REFERENCES

Aghaloo, T. L., Chaichanasakul, T., Bezouglaia, O., Kang, B., Franco, R., Dry, S. M., … Tetradis, S. (2010). Osteogenic potential of mandibular vs. long-bone marrow stromal cells. *Journal of Dental Research*, *89*(11), 1293–1298. https://doi.org/10.1177/0022034510378427

Akintoye, S. O., Giavis, P., Stefanik, D., Levin, L., & Mante, F. K. (2008). Comparative osteogenesis of maxilla and iliac crest human bone marrow stromal cells attached to oxidized titanium: A pilot study. *Clinical Oral Implants Research*, *19*(11), 1197–1201. https://doi.org/10.1111/j.1600-0501.2008.01592.x

Akintoye, S. O., Lam, T., Shi, S., Brahim, J., Collins, M. T., & Robey, P. G. (2006). Skeletal site-specific characterization of orofacial and iliac crest human bone marrow stromal cells in same individuals. *Bone*, *38*(6), 758–768. https://doi.org/10.1016/j.bone.2005.10.027

Al-Ahmady, H. H., Abd Elazeem, A. F., Bellah Ahmed, N. E., Shawkat, W. M., Elmasry, M., Abdelrahman, M. A., & Abderazik, M. A. (2018). Combining autologous bone marrow mononuclear cells seeded on collagen sponge with Nano Hydroxyapatite, and platelet-rich fibrin: Reporting a novel strategy for alveolar cleft bone regeneration. *Journal of Cranio-Maxillofacial Surgery*, *46*(9), 1593–1600. https://doi.org/10.1016/j.jcms.2018.05.049

Baglio, S. R., Rooijers, K., Koppers-Lalic, D., Verweij, F. J., Perez Lanzon, M., Zini, N., … Pegtel, D. M. (2015). Human bone marrow- and adipose-mesenchymal stem cells secrete exosomes enriched in distinctive miRNA and tRNA species. *Stem Cell Research & Therapy*, *6*(1), https://doi.org/10.1186/s13287-015-0116-z

Bajaj, A. K., Wongworawat, A. A., & Punjabi, A. (2003). Management of alveolar clefts. *Journal of Craniofacial Surgery*, *14*(6), 840–846. https://doi.org/10.1097/00001665-200311000-00005

Barbero-Becerra, V. J., Giraudi, P. J., Chavez-Tapia, N. C., Uribe, M., Tiribelli, C., & Rosso, N. (2015). The interplay between hepatic stellate cells and hepatocytes in an in vitro model of NASH. *Toxicology in Vitro*, *29*(7), 1753–1758. https://doi.org/10.1016/j.tiv.2015.07.010

Benlidayi, M. E., Tatli, U., Kurkcu, M., Uzel, A., & Oztunc, H. (2012). Comparison of bovine-derived hydroxyapatite and autogenous bone for secondary alveolar bone grafting in patients with alveolar clefts. *Journal of Oral and Maxillofacial Surgery*, *70*(1), e95–e102. https://doi.org/10.1016/j.joms.2011.08.041

Bissell, M. J., & Radisky, D. (2001). Putting tumours in context. *Nature Reviews Cancer*, *1*(1), 46–54. https://doi.org/10.1038/35094059

Bobrie, A., Colombo, M., Raposo, G., & Thery, C. (2011). Exosome secretion: Molecular mechanisms and roles in immune responses. *Traffic*, *12*(12), 1659–1668. https://doi.org/10.1111/j.1600-0854.2011.01225.x

Chai, Y., Jiang, X., Ito, Y., Bringas, P. Jr, Han, J., Rowitch, D. H., … Sucov, H. M. (2000). Fate of the mammalian cranial neural crest during tooth and mandibular morphogenesis. *Development*, *127*(8), 1671–1679

Chai, Y., & Maxson Jr, R. E. (2006). Recent advances in craniofacial morphogenesis. *Developmental Dynamics*, *235*(9), 2353–2375. https://doi.org/10.1002/dvdy.20833

Cho-Lee, G. Y., Garcia-Diez, E. M., Nunes, R. A., Marti-Pages, C., Sieira-Gil, R., & Rivera-Baro, A. (2013). Review of secondary alveolar cleft repair. *Annals of Maxillofacial Surgery*, *3*(1), 46–50. https://doi.org/10.4103/2231-0746.110083

Cooper, G. M., Mooney, M. P., Gosain, A. K., Campbell, P. G., Losee, J. E., & Huard, J. (2010). Testing the critical size in calvarial bone defects: Revisiting the concept of a critical-size defect. *Plastic and Reconstructive Surgery*, *125*(6), 1685–1692. https://doi.org/10.1097/PRS.0b013e3181cb63a3

Crespi, R., Vinci, R., Cappare, P., Gherlone, E., & Romanos, G. E. (2007). Calvarial versus iliac crest for autologous bone graft material for a sinus lift procedure: A histomorphometric study. *The International Journal of Oral & Maxillofacial Implants*, *22*(4), 527–532.

Cui, Y., Luan, J., Li, H., Zhou, X., & Han, J. (2016). Exosomes derived from mineralizing osteoblasts promote ST2 cell osteogenic differentiation by alteration of microRNA expression. *FEBS Letters*, *590*(1), 185–192. https://doi.org/10.1002/1873-3468.12024

de Souza Faloni, A. P., Schoenmaker, T., Azari, A., Katchburian, E., Cerri, P. S., de Vries, T. J., & Everts, V. (2011). Jaw and long bone marrows have a different osteoclastogenic potential. *Calcified Tissue International*, *88*(1), 63–74. https://doi.org/10.1007/s00223-010-9418-4

Fang, S., Li, Y., & Chen, P. (2019). Osteogenic effect of bone marrow mesenchymal stem cell-derived exosomes on steroid-induced

osteonecrosis of the femoral head. *Drug Design, Development and Therapy, 13*, 45–55. https://doi.org/10.2147/DDDT.S178698

Gao, Y., Connell, J. P., Wadhwa, L., Ruano, R., & Jacot, J. G. (2014). Amniotic fluid-derived stem cells demonstrated cardiogenic potential in indirect co-culture with human cardiac cells. *Annals of Biomedical Engineering, 42*(12), 2490–2500. https://doi.org/10.1007/s10439-014-1114-5

Gimbel, M., Ashley, R. K., Sisodia, M., Gabbay, J. S., Wasson, K. L., Heller, J., … Bradley, J. P. (2007). Repair of alveolar cleft defects: Reduced morbidity with bone marrow stem cells in a resorbable matrix. *Journal of Craniofacial Surgery, 18*(4), 895–901. https://doi.org/10.1097/scs.0b013e3180a771af

Guo, Z., Li, H., Li, X., Yu, X., Wang, H., Tang, P., & Mao, N. (2006). In vitro characteristics and in vivo immunosuppressive activity of compact bone-derived murine mesenchymal progenitor cells. *Stem Cells, 24*(4), 992–1000. https://doi.org/10.1634/stemcells.2005-0224

Helms, J. A., & Schneider, R. A. (2003). Cranial skeletal biology. *Nature, 423*(6937), 326–331. https://doi.org/10.1038/nature01656

Herberg, S., Susin, C., Pelaez, M., Howie, R. N., Moreno de Freitas, R., Lee, J., … Hill, W. D. (2014). Low-dose bone morphogenetic protein-2/ stromal cell-derived factor-1beta cotherapy induces bone regeneration in critical-size rat calvarial defects. *Tissue Engineering. Part A, 20*(9–10), 1444–1453. https://doi.org/10.1089/ten.TEA.2013.0442

Huang, C. C., Narayanan, R., Alapati, S., & Ravindran, S. (2016). Exosomes as biomimetic tools for stem cell differentiation: Applications in dental pulp tissue regeneration. *Biomaterials, 111*, 103–115. https://doi.org/10.1016/j.biomaterials.2016.09.029

Huang, Y., Zheng, Y., Jia, L., & Li, W. (2015). Long noncoding RNA H19 promotes osteoblast differentiation Via TGF-beta1/Smad3/HDAC signaling pathway by deriving miR-675. *Stem Cells, 33*(12), 3481–3492. https://doi.org/10.1002/stem.2225

Huang, Y., Zheng, Y., Jin, C., Li, X., Jia, L., & Li, W. (2016). Long Non-coding RNA H19 inhibits adipocyte differentiation of bone marrow mesenchymal stem cells through epigenetic modulation of histone deacetylases. *Scientific Reports, 6*(1), https://doi.org/10.1038/srep28897

Ichiyanagi, T., Anabuki, K., Nishijima, Y., & Ono, H. (2010). Isolation of mesenchymal stem cells from bone marrow wastes of spinal fusion procedure (TLIF) for low back pain patients and preparation of bone dusts for transplantable autologous bone graft with a serum glue. *Bioscience Trends, 4*(3), 110–118.

Jiang, N., Xiang, L., He, L., Yang, G., Zheng, J., Wang, C., … Mao, J. J. (2017). Exosomes mediate epithelium-mesenchyme crosstalk in organ development. *ACS Nano, 11*(8), 7736–7746. https://doi.org/10.1021/acsnano.7b01087

Johnstone, R. M., Adam, M., Hammond, J. R., Orr, L., & Turbide, C. (1987). Vesicle formation during reticulocyte maturation. Association of plasma membrane activities with released vesicles (exosomes). *The Journal of Biological Chemistry, 262*(19), 9412–9420.

Kalimuthu, S., Gangadaran, P., Rajendran, R. L., Zhu, L., Oh, J. M., Lee, H. W., … Ahn, B. C. (2018). A new approach for loading anticancer drugs into mesenchymal stem cell-derived exosome mimetics for cancer therapy. *Frontiers in Pharmacology, 9*, 1116. https://doi.org/10.3389/fphar.2018.01116

Kim, J. W., Wieckowski, E., Taylor, D. D., Reichert, T. E., Watkins, S., & Whiteside, T. L. (2005). Fas ligand-positive membranous vesicles isolated from sera of patients with oral cancer induce apoptosis of activated T lymphocytes. *Clinical Cancer Research, 11*(3), 1010–1020.

Koole, R., Bosker, H., & van der Dussen, F. N. (1989). Late secondary autogenous bone grafting in cleft patients comparing mandibular (ectomesenchymal) and iliac crest (mesenchymal) grafts. *Journal of Cranio-Maxillofacial Surgery, 17*(Suppl. 1), 28–30. https://doi.org/10.1016/S1010-5182(89)80036-8

Krebsbach, P. H., Mankani, M. H., Satomura, K., Kuznetsov, S. A., & Robey, P. G. (1998). Repair of craniotomy defects using bone

marrow stromal cells. *Transplantation, 66*(10), 1272–1278. https://doi.org/10.1097/00007890-199811270-00002

Lan, W. R., Pan, S., Li, H. Y., Sun, C., Chang, X., Lu, K., … Li, C. Q. (2019). Inhibition of the notch1 pathway promotes the effects of nucleus pulposus cell-derived exosomes on the differentiation of mesenchymal stem cells into nucleus pulposus-like cells in rats. *Stem Cells International, 2019*, 1–12. https://doi.org/10.1155/2019/8404168

Lee, J. T., Choi, S. Y., Kim, H. L., Kim, J. Y., Lee, H. J., & Kwon, T. G. (2015). Comparison of gene expression between mandibular and iliac bone-derived cells. *Clinical Oral Investigations, 19*(6), 1223–1233. https://doi.org/10.1007/s00784-014-1353-8

Li, B., Xu, H., Han, H., Song, S., Zhang, X., Ouyang, L., … Zhuang, W. (2018). Exosome-mediated transfer of lncRUNX2-AS1 from multiple myeloma cells to MSCs contributes to osteogenesis. *Oncogene, 37*(41), 5508–5519. https://doi.org/10.1038/s41388-018-0359-0

Mackie, E. J., Ahmed, Y. A., Tatarczuch, L., Chen, K. S., & Mirams, M. (2008). Endochondral ossification: How cartilage is converted into bone in the developing skeleton. *The International Journal of Biochemistry & Cell Biology, 40*(1), 46–62. https://doi.org/10.1016/j.biocel.2007.06.009

Mathivanan, S., Ji, H., & Simpson, R. J. (2010). Exosomes: Extracellular organelles important in intercellular communication. *Journal of Proteomics, 73*(10), 1907–1920. https://doi.org/10.1016/j.jprot.2010.06.006

Matsubara, T., Suardita, K., Ishii, M., Sugiyama, M., Igarashi, A., Oda, R., … Kato, Y. (2005). Alveolar bone marrow as a cell source for regenerative medicine: Differences between alveolar and iliac bone marrow stromal cells. *Journal of Bone and Mineral Research, 20*(3), 399–409. https://doi.org/10.1359/JBMR.041117

Mikoya, T., Inoue, N., Matsuzawa, Y., Totsuka, Y., Kajii, T. S., & Hirosawa, T. (2010). Monocortical mandibular bone grafting for reconstruction of alveolar cleft. *The Cleft Palate-Craniofacial Journal, 47*(5), 454–468. https://doi.org/10.1597/09-172

Mimeault, M., Hauke, R., & Batra, S. K. (2007). Stem cells: A revolution in therapeutics-recent advances in stem cell biology and their therapeutic applications in regenerative medicine and cancer therapies. *Clinical Pharmacology & Therapeutics, 82*(3), 252–264. https://doi.org/10.1038/sj.clpt.6100301

Moreau, J. L., Caccamese, J. F., Coletti, D. P., Sauk, J. J., & Fisher, J. P. (2007). Tissue engineering solutions for cleft palates. *Journal of Oral and Maxillofacial Surgery, 65*(12), 2503–2511. https://doi.org/10.1016/j.joms.2007.06.648

Nwoku, A. L., Al Atel, A., Al Shlash, S., Oluyadi, B. A., & Ismail, S. (2005). Retrospective analysis of secondary alveolar cleft grafts using iliac of chin bone. *Journal of Craniofacial Surgery, 16*(5), 864–868. https://doi.org/10.1097/01.scs.0000179742.45424.0a

Ostrowski, M., Carmo, N. B., Krumeich, S., Fanget, I., Raposo, G., Savina, A., … Thery, C. (2010). Rab27a and Rab27b control different steps of the exosome secretion pathway. *Nature Cell Biology, 12*(1), 19–30; sup pp 11–13. https://doi.org/10.1038/ncb2000

Piecewicz, S., & Sengupta, S. (2011). The dynamic glycome microenvironment and stem cell differentiation into vasculature. *Stem Cells and Development, 20*(5), 749–758. https://doi.org/10.1089/scd.2010.0454

Poggio, M., Hu, T., Pai, C. C., Chu, B., Belair, C. D., Chang, A., … Blelloch, R. (2019). Suppression of exosomal PD-L1 induces systemic antitumor immunity and memory. *Cell, 177*(2), 414–427.e13. https://doi.org/10.1016/j.cell.2019.02.016

Record, M., Carayon, K., Poirot, M., & Silvente-Poirot, S. (2014). Exosomes as new vesicular lipid transporters involved in cell-cell communication and various pathophysiologies. *Biochimica Et Biophysica Acta, 1841*(1), 108–120. https://doi.org/10.1016/j.bbalip.2013.10.004

Thery, C., Ostrowski, M., & Segura, E. (2009). Membrane vesicles as conveyors of immune responses. *Nature Reviews Immunology, 9*(8), 581–593. https://doi.org/10.1038/nri2567

Valadi, H., Ekstrom, K., Bossios, A., Sjostrand, M., Lee, J. J., & Lotvall, J. O. (2007). Exosome-mediated transfer of mRNAs and microRNAs is a novel mechanism of genetic exchange between cells. *Nature Cell Biology*, *9*(6), 654–659. https://doi.org/10.1038/ncb1596

Xu, Q., Cui, Y., Luan, J., Zhou, X., Li, H., & Han, J. (2018). Exosomes from C2C12 myoblasts enhance osteogenic differentiation of MC3T3-E1 pre-osteoblasts by delivering miR-27a-3p. *Biochemical and Biophysical Research Communications*, *498*(1), 32–37. https://doi.org/10.1016/j.bbrc.2018.02.144

Ye, S., Seo, K. B., Park, B. H., Song, K. J., Kim, J. R., Jang, K. Y., … Lee, K. B. (2013). Comparison of the osteogenic potential of bone dust and iliac bone chip. *The Spine Journal*, *13*(11), 1659–1666. https://doi.org/10.1016/j.spinee.2013.06.012

Zhang, G., & Yang, P. (2018). A novel cell-cell communication mechanism in the nervous system: Exosomes. *Journal of Neuroscience Research*, *96*(1), 45–52. https://doi.org/10.1002/jnr.24113

Zheng, Y., Cai, J., Hutchins, A. P., Jia, L., Liu, P., Yang, D., … Wei, S. (2016). Remission for loss of odontogenic potential in a new micromilieu in vitro. *PLoS ONE*, *11*(4), e0152893. https://doi.org/10.1371/journal.pone.0152893

Zheng, Y., Li, X., Huang, Y., Jia, L., & Li, W. (2017). The circular RNA landscape of periodontal ligament stem cells during osteogenesis. *Journal of Periodontology*, *88*(9), 906–914. https://doi.org/10.1902/jop.2017.170078

SUPPORTING INFORMATION

Additional supporting information may be found online in the Supporting Information section at the end of the article.